Journal Name

ARTICLE TYPE

Cite this: DOI: 10.1039/xxxxxxxxxx

The ionic versus metallic nature of 2D electrides: A density-functional description

Stephen G. Dale,*[a] Erin R. Johnson[b]

Received Date
Accepted Date

DOI: 10.1039/xxxxxxxxxx

www.rsc.org/journalname

The two-dimensional (2D) electrides are a highly unusual class of matierals, possessing interstitial electron layers sandwiched between cationic atomic layers of the solid. In this work, density-functional theory, with the exchange-hole dipole moment dispersion correction, is used to investigate exfoliation and interlayer sliding of the only two experimentally known 2D electrides: $[Ca_2N]^+e^-$ and $[Y_2C]^{2+}(2e^-)$. Examination of the valence states during exfoliation identifies intercalated electrons in the bulk and weakly-bound surface-states in the fully-expanded case. The calculated exfoliation energies for the 2D electrides are found to be much higher than for typical 2D materials, which is attributed to the ionic nature of the electrides and the strong Coulomb forces governing the interlayer interactions. Conversely, the calculated sliding barriers are found to be quite low, comparable to those for typical 2D materials, and are effectively unchanged by exclusion of dispersion. We conjecture that the metallic nature of the interstitial electrons allows the atomic layers to move relative to each other without significantly altering the interlayer binding. Finally, comparison with previous works reveals the importance of a system-dependent dispersion correction in the density-functional treatment.

Introduction

The discovery, ongoing characterisation, and potential applications of 2D materials have had a profound impact on the scientific community in recent years. Well-characterised 2D materials such as graphene, boron nitride (BN), and molybdenum disulfide (MoS_2) possess low barriers for exfoliation[1] and lateral layer motion,[2] among other attractive properties. Graphene in particular has been described as, 'one of the most promising materials for post-silicon electronics'.[3] Upon the identification of 2D electrides,[4,5] studies looking for similar desirable electronic and mechanical properties swiftly followed.

Electrides are ionic crystals in which the anions are stoichiometrically replaced with localised electrons.[6] The first electrides discovered used alkali metal-ligand complexes involving electron-rich, organic ring- and cage-like ligands that allow the valence electron to dissociate from, and exist independently of, the complex.[7–15] These materials were highly sensitive to both temperature and atmosphere, which hindered research and application efforts. In 2003,[16] the first inorganic electride, $[Ca_{24}Al_{28}O_{64}]^{4+}(4e^-)$, was identified and shown to be stable at temperatures up to 1600 °C.[17] This was a significant increase in thermal stability compared to the most-stable organic electride (which decomposes at 40°C[14]) and allowed development of a series of potential applications.[18–23]

In recent years a number of new inorganic electrides have been identified.[4,5,24,25] Two of these materials, $[Ca_2N]^+e^-$ and $[Y_2C]^{2+}(2e^-)$, possess covalently-bonded 2D atomic layers with the 'electride' electrons intercalated between each layer.[4,5] It was hypothesised and theoretically demonstrated that a layer of $[Ca_2N]^+e^-$ could be separated from the bulk material, similar to the exfoliation of graphene sheets.[26] The 'electride' electrons are then predicted to dissociate above and below the surface of the exfoliated layer, forming a pseudo-2D free-electron gas. Stable exfoliation of $[Ca_2N]^+e^-$ was recently verified experimentally[27] and introduces a whole new range of potential applications for electride materials. Theoretical studies have also predicted that a $[Y_2C]^{2+}(2e^-)$ monolayer would be strong enough to be free standing,[28] but harder to exfoliate than $[Ca_2N]^+e^-$.[29]

Theoretical calculations[29,30] revealed a low energy barrier of 1.6 meV Å^{-2} to interlayer sliding of $[Ca_2N]^+e^-$. This prompted the suggestion that more facile exfoliation of $[Ca_2N]^+e^-$ layers could be achieved by a combination of such sliding and electron doping;[29] peripheral experimental observations seem consistent with this suggestion.[27] Moreover, the predicted sliding barrier is low enough to make the 2D electrides excellent candidates for new solid lubricants. The current, primary failure of solid lubricants is a lack of atmospheric stability as the temperature in-

[a] Department of Chemistry, Dalhousie University, 6274 Coburg Rd, P.O.Box 15000 B3H 4R2, Halifax, Nova Scotia, Canada E-mail: stephen.dale@dal.ca
[b] Department of Chemistry, Dalhousie University, 6274 Coburg Rd, P.O.Box 15000 B3H 4R2, Halifax, Nova Scotia, Canada E-mail: erin.johnson@dal.ca

creases, and unfortunately, this is currently a flaw that the 2D electrides share. However, a recent computational study predicted the existence of another 24 potential 2D electrides.[31] If even a fraction of those predictions are correct, the electride field would expand dramatically and could overcome problems faced by the limited sample space of stable electride crystals.

In this work we use density-functional theory (DFT) and the exchange-hole dipole moment (XDM)[32,33] dispersion model to examine exfoliation and interlayer sliding energies of the $[Ca_2N]^+e^-$ and $[Y_2C]^{2+}(2e^-)$, the only experimentally characterised 2D electrides. This is the first study to apply a non-empirical, density-dependent dispersion correction to the 2D electrides, allowing the dispersion coefficients to respond to changes in the electronic structure of the system under study. Comparison between the present results and previous studies reveal large exfoliation energy differences caused primarily by the lack of, or choice of, dispersion correction; these differences and their impact on the computed properties is discussed in detail in section 3.3. Additionally, we present the first study of the evolution of the 'electride' states as exfoliation occurs and observe the transition from interstitial layers to surface states. The first sliding calculations for $[Y_2C]^{2+}(2e^-)$ and the first dispersion-corrected results for sliding of $[Ca_2N]^+e^-$ are also presented. The results reveal that the 2D electrides have the unique combination of strong interlayer binding during exfoliation, but weak interlayer interactions during sliding, when compared to other common 2D materials. The former is explained by the ionic nature of the materials, with Coulomb attraction between the positively-charged atomic layers and negatively-charged interstitial electrons, leading to a high exfoliation energy. The latter is explained by the metallic nature of the interstitial electron density, resulting in nearly non-directional interlayer interactions.

Computational Methods

Unit-cell geometries of $[Ca_2N]^+e^-$ [4,34] and $[Y_2C]^{2+}(2e^-)$ [5,35,36] were taken directly from their experimental crystal structures. Full relaxation of the atomic positions and cell dimensions under periodic boundary conditions was performed using the B86bPBE functional[37,38] and the XDM dispersion model[33,39,40] with the Quantum Espresso program.[41] Unless specified otherwise, calculations presented in this work used the planewave/pseudopotentials (PW/PS) approach and the Projector Augmented Wave (PAW) formalism,[42] with a plane-wave cutoff energy of 100 Ry, a $12\times12\times12$ $\boldsymbol{k}$-point mesh, and cold smearing[43] at a temperature of 0.01 Ry. Pseudopotentials were adapted from the atompaw library.[44]

Interlayer-sliding calculations were conducted by fixing the unit-cell parameters and the x, y coordinates for all atoms after the desired lateral shift for a single layer; the z-coordinates of each atom were then allowed to relax. Exfoliation calculations were conducted by shifting each layer in the z-direction, such that all layers remained equidistant; unit-cell parameters were adjusted to accommodate this. At a given separation, the z-parameter of the unit-cell and z-coordinate of all the atoms were held fixed and the x,y cell parameters and atomic coordinates were allowed to relax.

Spin-polarised calculations were attempted with a variety of initial magnetic-bias motifs in the spirit of our previous work.[45] However, these calculations would consistently return spin-unpolarised solutions or, in the few cases when a magnetic state for $[Y_2C]^{2+}(2e^-)$ was found, it was higher in energy than the spin-unpolarised solution. Consequently, all of the calculations presented herein do not include spin-polarisation.

Results and Discussion

Exfoliation

Our calculations predict exfoliation energies of 94.9 and 145.6 meV Å^{-2} for $[Ca_2N]^+e^-$ and $[Y_2C]^{2+}(2e^-)$, respectively. The potential energy surfaces from which these values are derived are shown in Figure 1. These exfoliation energies are significantly larger than for the more common 2D materials graphite, BN, and MoS_2, calculated to be 21.0, 21.6, and 23.2 meV Å^{-2}, respectively, calculated using identical methods and consistent with previous work.[46] Interlayer binding of graphite, BN, or MoS_2 is primarily due to dispersion forces, while the binding in the 2D electrides is primarily due to electrostatic forces between the positively-charged atomic layers and negatively-charged intercalated electrons. Indeed, even if the XDM dispersion energy is removed, the exfoliation energies of the electrides remain high, at 61.8 and 98.2 meV Å^{-2} for $[Ca_2N]^+e^-$ and $[Y_2C]^{2+}(2e^-)$, respectively. Comparison with other common 2D materials reveals roughly equivalent XDM contributions to the exfoliation energy of 33.1, 47.7, 28.5, 28.9 and 31.2 meV Å^{-2} for $[Ca_2N]^+e^-$, $[Y_2C]^{2+}(2e^-)$, graphene, BN and MoS_2, respectively. However, the dispersion contribution is much more significant for the traditional 2D materials as it is the single force responsible for interlayer binding. The 2D electride layers are already bound by electrostatic forces and the inclusion of dispersion only serves to increase their stability.

Fig. 1 Computed potential energy surfaces for exfoliation of the $[Ca_2N]^+e^-$ (red) and $[Y_2C]^{2+}(2e^-)$ (black) electrides. Interlayer separation is measured as the vertical distance between metal atoms on neighbouring layers, consistent with previous studies.[29]

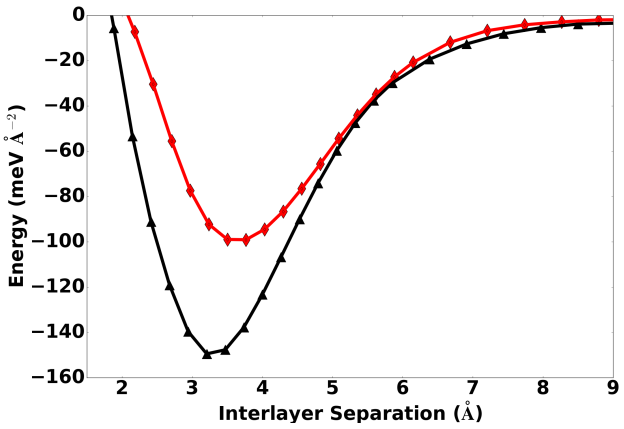

Perhaps the simplest way to understand the difference between the exfoliation energies of the two electrides is through

examination of the oxidation numbers. The oxidation states in $[Y_2C]^{2+}(2e^-)$ are 3+ for Y and 4- for C, whose magnitudes are higher by one compared to the corresponding values of 2+ for Ca and 3- for N in $[Ca_2N]^+e^-$. In light of this, the higher exfoliation energy of $[Y_2C]^{2+}(2e^-)$ is due to the increased electrostatic attraction resulting from the more positive charge for the metal atoms at the surface of each layer and the greater number of interstitial electrons, consistent with the higher base-functional contribution to the exfoliation barrier.

Figure 2 shows density plots for the valence or 'electride' state[47,48] for each material as the interlayer separation is gradually increased from the potential-energy minima to the asymptotic energy limit. Specifically, the electron density of all states from 0.25 eV below and up to the Fermi level is plotted. This threshold was chosen to ensure only the highest-lying valence states were consistently represented and the resulting valence densities were renormalized for all interlayer separations. These plots reveal a higher valence electron density between each layer for $[Y_2C]^{2+}(2e^-)$, in line with the higher number of 'electride' electrons in the stoichiometric formula. Figure 2 also reveals the transition of the 'electride' electrons from an interstitial state at the potential energy minima (leftmost frame) to a surface state at the asymptotic separation limit (rightmost frame). This surface state was first predicted to exist for an isolated layer of $[Ca_2N]^+e^-$,[26] with localisation of electron density above and below the atomic layer allowing formation of what is effectively a 2D free-electron gas. Figure 2 predicts that this state also exists for $[Y_2C]^{2+}(2e^-)$.

The behaviour of the valence state throughout exfoliation is markedly different for each electride. The $[Ca_2N]^+e^-$ valence state is initially intercalated between each atomic layer and gradually becomes more disperse with increasing separation, eventually splitting into surface states at the edge of each layer. The $[Y_2C]^{2+}(2e^-)$ valence state is initially very well localised between each layer. Indeed, non-nuclear maxima in the electron density were identified and are consistent with the regions of high density in the valence state for the equilibrium geometry of $[Y_2C]^{2+}(2e^-)$. As the material is exfoliated, the intercalated electron initially retreats back to, and disperses over, the atomic layer. The valence state only returns to the surface of each atomic layer at very large interlayer separations, approaching the asymptotic energy limit.

Note that any examination of electron densities generated using Generalised Gradient Approximations (GGAs), such as PBE or B86bPBE, should be treated with caution due to delocalisation error inherent to these methods.[49–56] This error is the source of many failings of semilocal density functionals including underestimation of band gaps, overstabilization of fractional charges, overestimation of charge transfer and polarizabilities, and underestimation of reaction barrier heights.[57–71] Inclusion of exact (Hartree-Fock) exchange, as in hybrid[72,73] long-range corrected[74–78]functionals can help mitigate this error,[62,79–86] but is generally intractable for planewave/pseudopotential calculations. However, as the name suggests, delocalisation error typically results in an overly disperse electron density. Indeed, examination of the Kevan solvated-electron model, an electride analogue consisting of six octahedrally-oriented water molecules that localise an excess electron, revealed this to be the case.[87] We expect similar behaviour for the electride systems examined in this work. Consequently, if one could correct for delocalisation error in the present calculations, we would expect the valence densities in Figure 2 to show greater density in the interstitial regions initially. On exfoliation, the surface states would be expected to contract, being more tightly bound to the atomic layers.

Interlayer Sliding

Figure 3 shows the 2D potential energy surfaces for sliding a single layer of either $[Ca_2N]^+e^-$ or $[Y_2C]^{2+}(2e^-)$ in the bulk crystal. At the minimum-energy points of the potential, the metal atoms of neighbouring layers are as far from each other as possible. At the maximum-energy points, the metal atoms of the translated layer align with the metal atoms of the neighbouring layers. Sliding barriers are calculated to be 2.7 and 5.6 meV $Å^{-2}$ for $[Ca_2N]^+e^-$ and $[Y_2C]^{2+}(2e^-)$, respectively. As in the previous section, stronger interlayer interactions in $[Y_2C]^{2+}(2e^-)$, justified by the oxidation states of the metal atoms at the surface of each layer (viz. 2+ for Ca and 3+ for Y). As sliding occurs, the metal atoms in neighbouring layers will approach each other and naturally the species with the higher charge will generate greater electrostatic repulsion, hence the higher sliding barrier for $[Y_2C]^{2+}(2e^-)$.

Note that the calculations used to generate Figure 3 assumed that the interlayer separation of the 2D electrides remains constant during sliding. To test the validity of this assumption, the lattice constant and atomic positions for each electride at the maximum-energy point along the sliding path were allowed to relax in the z-direction. This causes the interlayer separation to increase from the equilibrium distances of 3.50 and 3.21 Å to 3.58 and 3.30 Å, for $[Ca_2N]^+e^-$ and $[Y_2C]^{2+}(2e^-)$, respectively. If this change in interlayer separation is taken into account, the sliding barriers are further reduced to 1.4 and 4.0 meV $Å^{-2}$, for $[Ca_2N]^+e^-$ and $[Y_2C]^{2+}(2e^-)$, respectively.

The dependence of the sliding barrier on the interlayer separation is examined further in Figure 4, which plots the sliding energy barrier for interlayer distances about the equilibrium geometry. The sliding barrier increases as the interlayer separation decreases, consistent with tribological studies which observe a linear increase in friction with applied load for common 2D materials.[88–91] Also, Figure 4 shows that our results are consistent with the previous work from Yi *et al.*[29,30], who predicted a sliding barrier of 1.6 meV $Å^{-2}$ for $Ca_2N]^+e^-$ at an interlayer separation of 3.87 Å, with the PBE functional.[38] Their predicted equilibrium interlayer separation was larger than in the present work due to neglect of dispersion.

Fig. 2 Plots of the renormalised valence-state electron density for $[Ca_2N]^+e^-$ (top) and $[Y_2C]^{2+}(2e^-)$ (bottom). Each sub-plot shows the valence density (e bohr^{-3}) within the (110) unit-cell plane bisecting the electride layers, with the x- and y-axes corresponding to the position within this plane. The plots are ordered from left to right according to increasing interlayer separation. The unit cells and chemical structures are shown to the left side of each plot. Atom colors are: Ca, white; N, blue; Y, grey; and C, black. Results are presented for six interlayer separations, ranging from the potential-energy minimum (left) to near the asymptotic energy limit (right). The specific interlayer separation is reported below each valence-density plot.

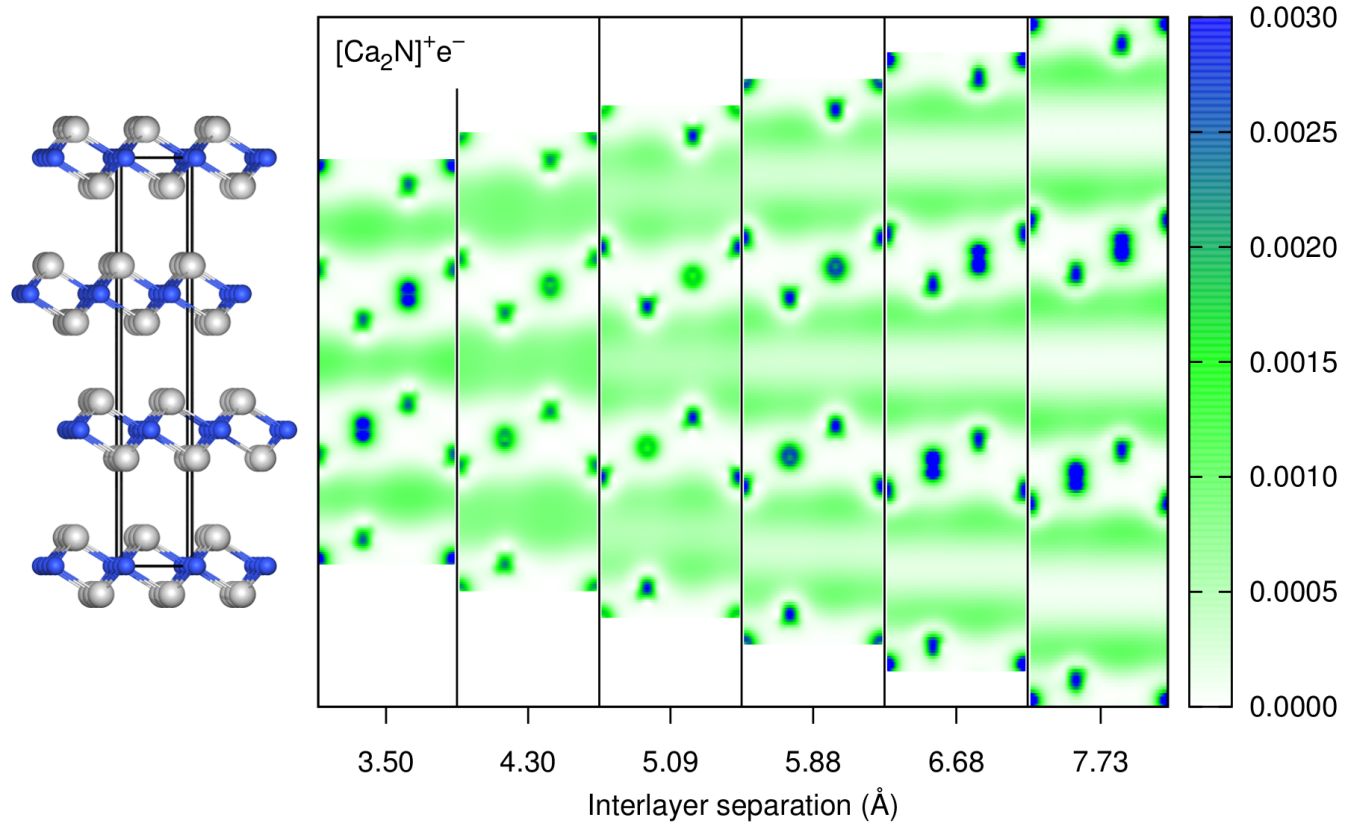

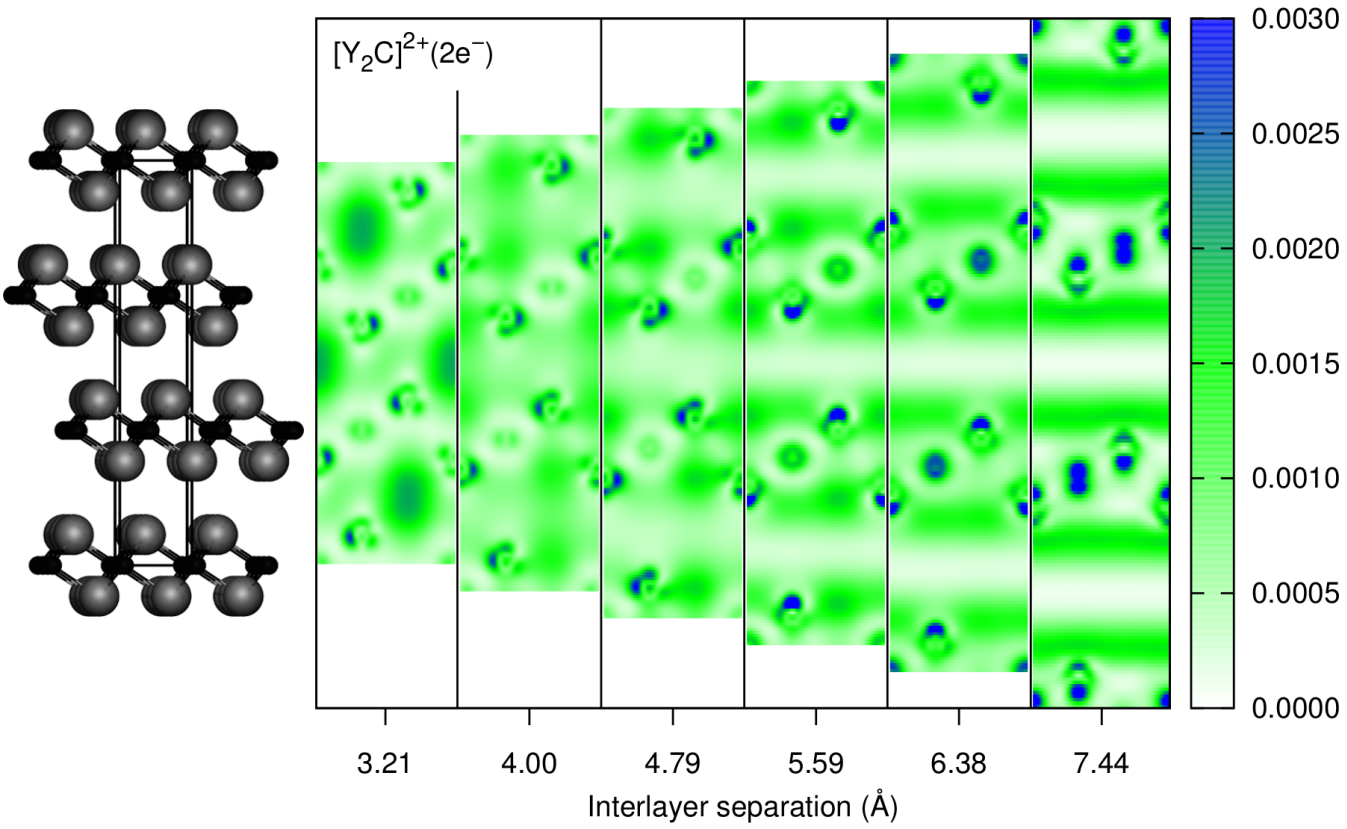

The sliding barriers of the 2D electrides calculated in this work are on par with equivalent energies for graphene, BN, and MoS_2, calculated to be 1.6, 2.0, and 4.7 meV Å^{-2}, respectively,[2,92] using PW86PBE-XDM.[38,93] Thus, 2D electrides would be good candidates for new solid lubricants if not for their high sensitivity to oxidative environments. Nonetheless, electrides do still show promise; a water-stable electride, $[Y_5Si_3]^+e^-$ was recently synthesised[25] and the existence of 24 new, stable 2D-electride crystal structures computationally predicted,[31] some of which may prove more resistant to oxidation.

Figure 4 also shows that, for a given geometry, the sliding barriers calculated with and without the XDM dispersion correction are roughly equivalent. Indeed the XDM-corrected barriers are slightly lower than those calculated using the base functional alone. This implies that dispersion forces do not play a significant role in interlayer sliding, in sharp contrast to the typical solid lubricants, graphite, BN, and MoS_2, where the dispersion energy is the principle component of the sliding barrier.[2,94]

We conjecture that the low sliding barriers for the 2D electrides are due to the non-directional metallic nature of the interstitial electron, as reflected in the valence density plots in Figure 2. While other 2D materials must overcome more directional van der Waals contacts for sliding to occur, the presence of the intercalated electron layer allows translation of the atomic structure without significantly impacting the stability of the system. This is consistent with early descriptions of electrides as 'expanded metals'[95] and recent observations that the band structure of the 2D electrides are independent of the stacking motifs between layers.[29]

The Role of Dispersion

Previously reported exfoliation energies for $[Ca_2N]^+e^-$ are 68.0,[26,30] 69.3[27,30] and, most recently, 63.0[29,30] meV Å^{-2}. Each of these calculations used the PBE[38] functional and the former two energies include the DFT-D2 dispersion correction.[96] The only other reported exfoliation energy for $[Y_2C]^{2+}(2e^-)$ is 96.0 meV Å^{-2} using only the PBE functional.[29,30] Our own reported values (94.9 and 145.6 meV Å^{-2} for $[Ca_2N]^+e^-$ and $[Y_2C]^{2+}(2e^-)$, respectively) are higher in every case. For comparison, calculations with the non-local optB86b-vdW functional[97] give exfoliation energies of 76.4 meV Å^{-2} for $[Ca_2N]^+e^-$ and 117.5 meV Å^{-2} for $[Y_2C]^{2+}(2e^-)$, which are also significantly higher than the previous results.

Figure 5 shows potential energy surfaces for $[Ca_2N]^+e^-$ and $[Y_2C]^{2+}(2e^-)$ calculated with and without the XDM dispersion correction. Removing the XDM dispersion correction from the exfoliation energies reported in this work gives 61.8 and 98.2 meV Å^{-2} for $[Ca_2N]^+e^-$ and $[Y_2C]^{2+}(2e^-)$, respectively, very closely reproducing the PBE results of Yi *et al.*[29] Clearly the increased exfoliation energies reported in this work are due to the dispersion correction applied. The difference between the XDM and DFT-D2 dispersion corrections is more subtle. Both XDM and DFT-D2 dispersion models use the first term in the series expansion,

$$E_{disp} = -\sum_{i<j} \frac{C_{6,ij}}{R_{ij}^6}, \tag{1}$$

as the primary contribution to the dispersion energy (although XDM also includes higher order C_8 and C_{10} terms). In this equation, the summation runs over all pair of atoms, i and j, and the R_{ij} are the interatomic separations. The primary difference between the two dispersion corrections is in the calculation of the atomic dispersion coefficients, $C_{6,ij}$.

DFT-D2 approximates the homoatomic dispersion coefficients as constant values calculated using the free-atomic ionisation potential (I) and polarisability (α_{free}) obtained with the PBE0[98] functional.[96]

$$C_{6,ii} = 0.05 N I_i \alpha_{i,free} \tag{2}$$

The parameter N has value 10 for 2nd-row elements, 18 for 3rd-row elements, and 36 for 4th-row elements. Heteroatomic dispersion coefficients are obtained from a simple combination rule.[96] For the alkali and alkaline earth metals specifically, it was acknowledged that the difference between free-atom and bulk C_6 values was so large as to be problematic. As a compromise, rather than using the equation above, the C_6 values of the proceeding group 8 element and following group 3 element were averaged and used instead. This gives a homoatomic C_6 value of 187.4 a.u. for Ca.[96]

XDM non-empirically calculates the pairwise dispersion coefficients from the atom-in-molecule polarisabilities (α) and integrals involving the exchange-hole dipole moments (d_X) determined from the electron density of the system and related properties.

$$C_{6,ij} = \frac{\alpha_i \alpha_j \langle d_X^2 \rangle_i \langle d_X^2 \rangle_j}{\langle d_X^2 \rangle_i \alpha_j + \langle d_X^2 \rangle_j \alpha_i} \tag{3}$$

The XDM dispersion coefficients have been shown to be in good agreement with available atomic and molecular reference data[99] and are sensitive to changes in the local chemical environment.[100,101] Figure 6 shows the change in value of the homoatomic XDM C_6 coefficients for Ca and Y in $[Ca_2N]^+e^-$ and $[Y_2C]^{2+}(2e^-)$, respectively, as the interlayer separation is increased. The homoatomic C_6 dispersion coefficient ranges between 600-800 a.u. for Ca and the elevated exfoliation energy reported in this work is consistent with the much larger calcium C_6 calculated by XDM with respect to DFT-D2.

To ensure the XDM C_6 values are physically correct, we computed the C_6 dispersion coefficients of atomic and bulk Ca, which gave values of 2053 and 823.5 a.u., respectively. The calculated C_6 value for atomic Ca matches well with a number of previously-reported values, all roughly 2000 a.u.[102–110] While experimental determination of C_6 values in the bulk metal is not possible, calculated bulk C_6 values tend to be roughly half of the free-atom values for coinage metals,[101,111] and this is consistent with the C_6 value calculated for bulk Ca metal in this work. Finally, we note that previous calculations by our group comparing the C_6 values of bulk and surface metal atoms tend to observe a 30% increase in the latter case.[101] If the fully-exfoliated electride is considered to resemble a metal surface, this trend is reproduced with respect to the bulk 2D electride, as shown in Figure 6.

The changing C_6 coefficients calculated by the XDM model can only be caused by a change in the exchange-hole dipole moment (d_X) or atom-in-molecule polarisability (α) of calcium, based on

Fig. 3 Potential energy surfaces for sliding of a single layer of $[Ca_2N]^+e^-$ (left) and $[Y_2C]^{2+}(2e^-)$ (right) with respect to other layers within the bulk electrides. These plots were generated from calculations using a plane-wave cut-off energy of 60 Ry and a 4×4×4 ***k***-point mesh.

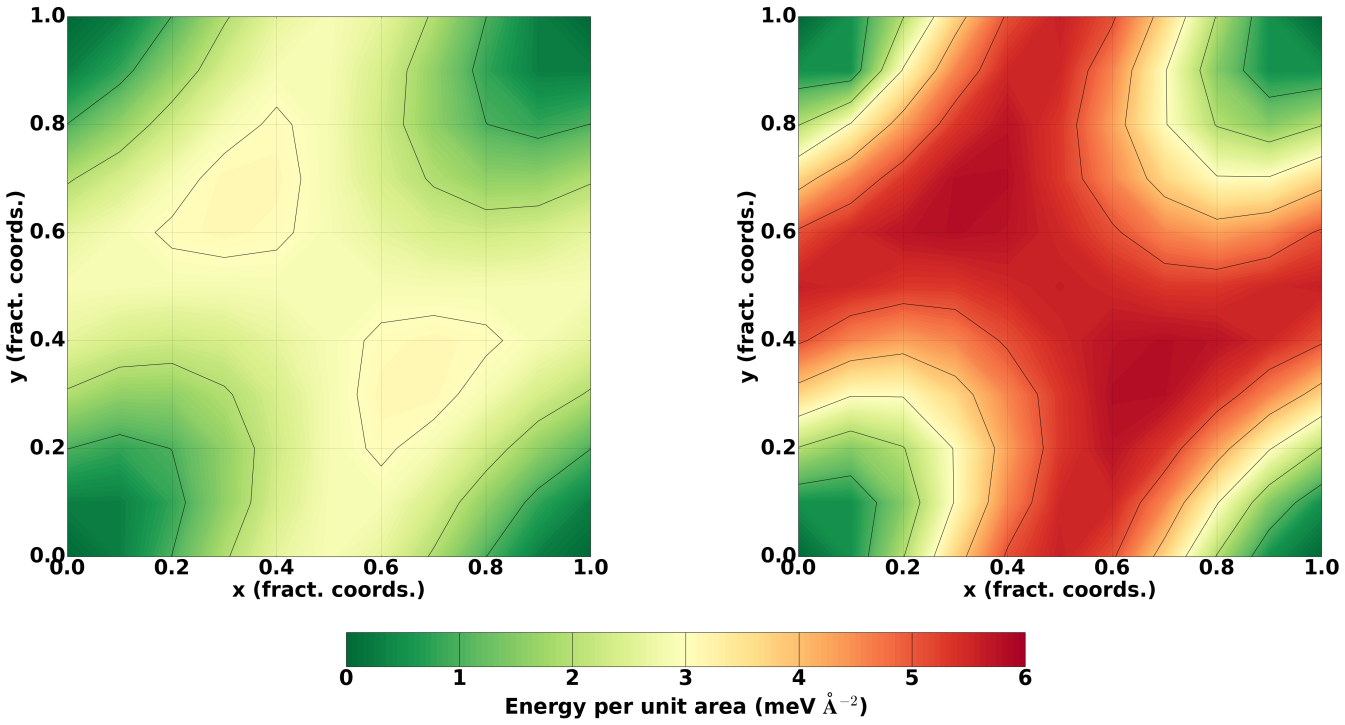

Equation 3. The evolution of d_X and α for Ca and Y are shown in Figure 6 and it is immediately obvious that the changes in d_X are the primary cause for the changes in the C_6 coefficients. This is consistent with previous studies of metal surfaces [101] and can be rationalised by considering the behaviour of the exchange-hole dipole moment of a free atom compared to an atom in a bulk metal. The exchange-hole of a free atom will remain centered on the nucleus regardless of the position of the reference electron, [112] resulting in large values of the exchange-hole dipole moment. Conversely, the exchange-hole of bulk metal remains close to the reference electron, [112] resulting in small values of the exchange-hole dipole moment. While the metal atoms in this work are neither free atoms nor bulk metals, the bulk 2D electride electron environment resembles that of a bulk metal, while the fully-exfoliated electride starts to take on some free-atom character.

While the changes in the metal-atom polarisabilities do not significantly impact the C_6 coefficients, they do reflect the change in the electron density within the 2D electrides as they are exfoliated and are consistent with previous observations in this work regarding Figure 2. The atomic polarisabilities are dependent on computed effective atomic volumes (V_i), such that

$$\alpha_i = \frac{V_i}{V_{i,free}} \alpha_{i,free}, \tag{4}$$

where $V_{i,free}$ is the effective free-atom volume and $\alpha_{i,free}$ is the free-atom polarisability. The atomic volumes are obtained from integrals involving the electron density (ρ),

$$V_i = \int w_i(\boldsymbol{r}) \rho(\boldsymbol{r}) r^3 d\boldsymbol{r}, \tag{5}$$

where the w_i are the Hirshfeld partitioning weights. [113] From Figure 6, the Ca atomic volume and polarisability in $[Ca_2N]^+e^-$ are minima at the equilibrium distance of of 3.5 Å and increase to maxima as the increasing interlayer separation causes the intercalated valence state to become more disperse. Upon sufficient separation, the valence states become surface states, causing the atomic volume and polarisability to decrease again. The Y atomic volume and polarisability in $[Y_2C]^{2+}(2e^-)$ do not reach minima until an interlayer separation of 4.27 Å, which is 1.26 Å larger than the equilibrium separation of 3.21 Å. This is consistent with the retreat of the valence state into the atomic layer. From this point onwards, the behaviour of V is consistent with $[Ca_2N]^+e^-$ as $[Y_2C]^{2+}(2e^-)$ separates into individual layers.

Conclusions

In this work, density-functional theory was applied to systematically examine the exfoliation and interlayer sliding properties of the 2D electride materials $[Ca_2N]^+e^-$ and $[Y_2C]^{2+}(2e^-)$. Plots of the valence density of each electride verify the increased electron density within the interstitial region of $[Y_2C]^{2+}(2e^-)$ compared to $[Ca_2N]^+e^-$. By examining changes in the valence density during exfoliation, we identify for the first time the transition between interstitial electron states in the bulk and previously-

Fig. 4 The sliding energy barrier as a function of interlayer separation for $[Ca_2N]^+e^-$ (left) and $[Y_2C]^{2+}(2e^-)$ (right). Both the dispersion-corrected (blue) and base-functional (green) results are shown. Please note the difference in scales.

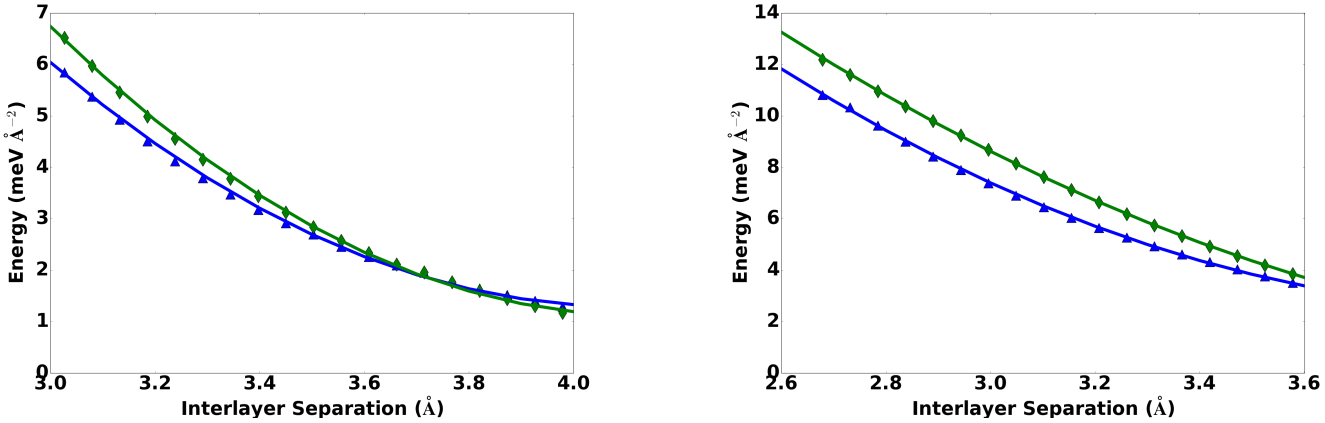

Fig. 5 Potential energy surfaces for exfoliation of $[Ca_2N]^+e^-$ (left) and $[Y_2C]^{2+}(2e^-)$ (right). Both the dispersion-corrected (blue) and base-functional (green) results are shown.

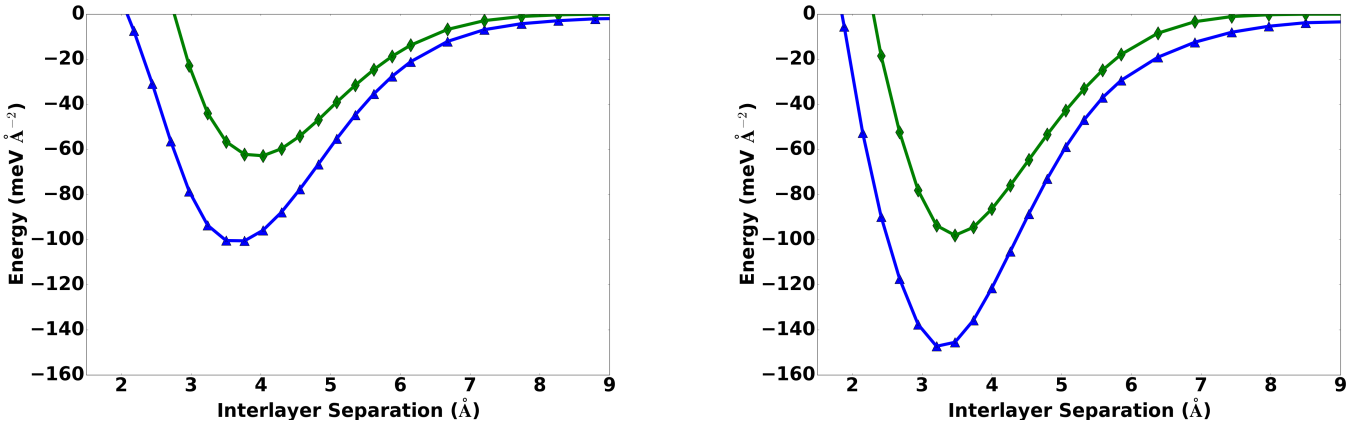

predicted surface states[26] for the separated atomic layers.

Comparison between this and previous dispersion-corrected DFT studies[26,29] reveals large differences in the computed exfoliation energies, primarily caused by the non-empirical versus empirical nature of the dispersion models used. Both the exfoliation energy and sliding barrier are found to be higher for $[Y_2C]^{2+}(2e^-)$ than for $[Ca_2N]^+e^-$, justified by greater electrostatic interactions in the former case due to the larger stoichiometric number of interstitial electrons and the higher oxidation state of the metal atoms.

The exfoliation energies of both materials were found to be considerably higher than those of other typical 2D materials, while the sliding barriers are comparable. We attribute this to the electride electrons acting as an intercalated anions in the former case, holding the layers together through coulomb attraction, rather than weaker van der Waals forces as is typical for 2D materials. In the latter case we suggest that the interstitial electron permits non-directional metallic bonding, allowing the individual layers to move relative to each other without significantly affecting their binding energy.

Finally, we note that the remarkable properties observed in this work should be consistent across other 2D electrides as they are due to the jointly ionic and metallic nature of the interactions, not the specific atomic composition or structure. If not for the atmospheric sensitivity of the 2D electrides, our calculations predict they would make excellent candidates for new solid lubricants. Despite this, the electride field continues to show promise with the recent discovery of an atmospherically-stable electride[25] and the highlighting of a large sample space of potential, new 2D electrides.[31]

Acknowledgements

The authors would like to acknowledge Dr. Alberto Otero-de-la-Roza for helpful discussions and technical support when using the critic2 program. We also thank the Natural Sciences and Engineering Research Council of Canada (NSERC) for financial support and the Multi-Environment Computer for Exploration and Discovery (MERCED), as well as Compute Canada (ACEnet and Westgrid), for computational time.

Fig. 6 Dependence of the calculated homoatomic C_6 dispersion coefficients (left), dipole moments (centre) and atomic polarisabilities (right) of Ca and Y in $[Ca_2N]^+e^-$ (red) and $[Y_2C]^{2+}(2e^-)$ (black) on the interlayer separation.

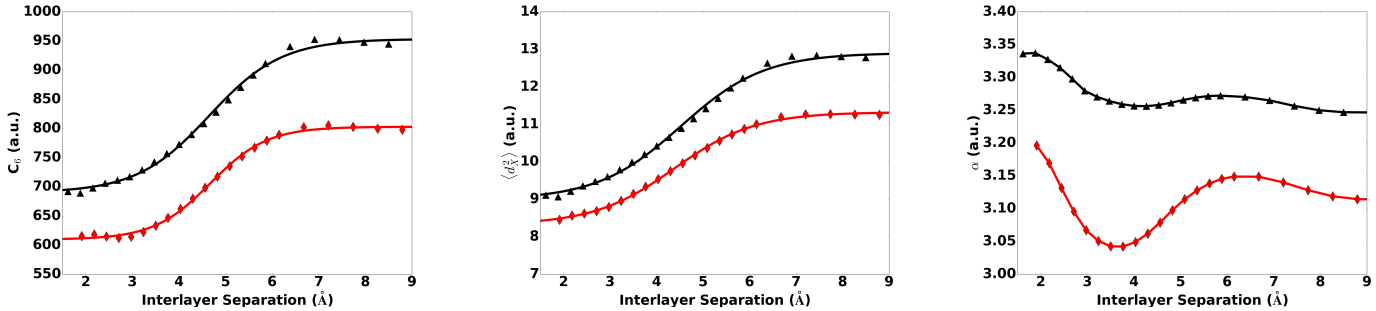

References

1 C. Li, T. Wang, Y. Wu, F. Ma, G. Zhao and X. Hao, *Nanotechnology*, 2014, **25**, 495302.

2 Z. Ye, A. Otero-De-La-Roza, E. R. Johnson and A. Martini, *Nanotechnology*, 2015, **26**, 165701.

3 T. Wehling, K. Novoselov, S. Morozov, E. Vdovin, M. Katsnelson, A. Geim and A. Lichtenstein, *Nano Lett.*, 2008, **8**, 173.

4 K. Lee, S. W. Kim, Y. Toda, S. Matsuishi and H. Hosono, *Nature*, 2013, **494**, 336.

5 X. Zhang, Z. Xiao, H. Lei, Y. Toda, S. Matsuishi, T. Kamiya, S. Ueda and H. Hosono, *Chemistry of Materials*, 2014, **26**, 6638.

6 J. L. Dye, *Accounts Chem. Res.*, 2009, **42**, 1564.

7 S. B. Dawes, D. L. Ward, R. H. Huang and J. L. Dye, *J. Am. Chem. Soc.*, 1986, **108**, 3534.

8 D. L. Ward, R. Huang and J. L. Dye, *Acta Crystallogr. C*, 1988, **44**, 1374.

9 D. L. Ward, R. Huang and J. L. Dye, *Acta Crystallogr C*, 1990, **46**, 1838.

10 S. B. Dawes, J. L. Eglin, K. J. Moeggenborg, J. Kim and J. L. Dye, *J. Am. Chem. Soc.*, 1991, **113**, 1605.

11 M. J. Wagner, R. H. Huang, J. L. Eglin and J. L. Dye, *Nature*, 1994, **368**, 726.

12 R. H. Huang, M. J. Wagner, D. J. Gilbert, K. A. Reidy-Cedergren, D. L. Ward, M. K. Faber and J. L. Dye, *J Am. Chem. Soc.*, 1997, **119**, 3765.

13 Q. Xie, R. H. Huang, A. S. Ichimura, R. C. Phillips, W. P. Pratt and J. L. Dye, *J. Am. Chem. Soc.*, 2000, **122**, 6971.

14 M. Y. Redko, J. E. Jackson, R. H. Huang and J. L. Dye, *J. Am. Chem. Soc.*, 2005, **127**, 12416.

15 S. G. Dale and E. R. Johnson, *Phys. Chem. Chem. Phys.*, 2017, **19**, 12819.

16 S. Matsuishi, Y. Toda, M. Miyakawa, K. Hayashi, T. Kamiya, M. Hirano, I. Tanaka and H. Hosono, *Science*, 2003, **301**, 626.

17 S. W. Kim, T. Shimoyama and H. Hosono, *Science*, 2011, **333**, 71.

18 S. Watanabe, T. Watanabe, K. Ito, N. Miyakawa, S. Ito, H. Hosono and S. Mikoshiba, *Sci. Technol. Adv. Mat.*, 2011, **12**, 034410.

19 Y. Toda, H. Hirayama, N. Kuganathan, A. Torrisi, P. V. Sushko and H. Hosono, *Nat. Commun.*, 2013, **4**, –.

20 H. Yanagi, K.-B. Kim, I. Koizumi, M. Kikuchi, H. Hiramatsu, M. Miyakawa, T. Kamiya, M. Hirano and H. Hosono, *J. Phys. Chem. C*, 2009, **113**, 18379.

21 M. Miyakawa, S. W. Kim, M. Hirano, Y. Kohama, H. Kawaji, T. Atake, H. Ikegami, K. Kono and H. Hosono, *J. Am. Chem. Soc.*, 2007, **129**, 7270.

22 J. Li, B. Yin, T. Fuchigami, S. Inagi, H. Hosono and S. Ito, *Electrochem. Commun.*, 2012, **17**, 52.

23 H. Buchammagari, Y. Toda, M. Hirano, H. Hosono, D. Takeuchi and K. Osakada, *Org. Lett.*, 2007, **9**, 4287.

24 Y. Zhang, Z. Xiao, T. Kamiya and H. Hosono, *J. Phys. Chem. Lett.*, 2015, **6**, 4966.

25 Y. Lu, J. Li, T. Tada, Y. Toda, S. Ueda, T. Yokoyama, M. Kitano and H. Hosono, *J. Am. Chem. Soc.*, 2016, **138**, 3970.

26 S. Zhao, Z. Li and J. Yang, *J. Am. Chem. Soc.*, 2014, **136**, 13313.

27 D. L. Druffel, K. L. Kuntz, A. H. Woomer, F. M. Alcorn, J. Hu, C. L. Donley and S. C. Warren, *J. Am. Chem. Soc.*, 2016, **138**, 16089.

28 J. Hou, K. Tu and Z. Chen, *J. Phys. Chem. C*, 2016, **120**, 18473.

29 S. Yi, J.-H. Choi, K. Lee, S. W. Kim, C. H. Park and J.-H. Cho, *Phys. Rev. B*, 2016, **94**, 235428.

30 To enable conversion to meV $Å^{-2}$, the cell parameters of the $[Ca_2N]^+e^-$ and $[Y_2C]^{2+}(2e^-)$ electrides calculated in this work were used if they were not given in the original work. For comparison, the difference in surface area between the expermental and optimized crystal structures of $[Ca_2N]^+e^-$ is calculated to be 7.1%. We consider this to be an upper limit to the error introduced by these unit conversions and it is small enough that the energy comparisons remain valid.

31 Y. Zhang, H. Wang, Y. Wang, L. Zhang and Y. Ma, *Phys. Rev. X*, 2017, **7**, 011017.

32 A. D. Becke and E. R. Johnson, *J. Chem. Phys.*, 2007, **127**, 154108.

33 E. R. Johnson, *Non-covalent Interactions in Quantum Chemistry and Physics*, Elsevier, 2017, ch. 5, pp. 215–248.

34 D. H. Gregory, A. Bowman, C. F. Baker and D. P. Weston, *J.*

Mater. Chem., 2000, **10**, 1635.
35 M. Atoji and M. Kikuchi, *J. Chem. Phys.*, 1969, **51**, 3863.
36 J. P. Maehlen, V. A. Yartys and B. C. Hauback, *J. Alloy. Compd.*, 2003, **351**, 151.
37 A. D. Becke, *J. Chem. Phys.*, 1986, **84**, 4524.
38 J. Perdew, K. Burke and M. Ernzerhof, *Phys. Rev. Lett.*, 1996, **77**, 3865.
39 A. Otero-de-la Roza and E. R. Johnson, *J. Chem. Phys.*, 2012, **136**, 174109.
40 A. Otero-de-la Roza and E. R. Johnson, *J. Chem. Phys.*, 2012, **137**, 054103.
41 P. Giannozzi, S. Baroni, N. Bonini, M. Calandra, R. Car, C. Cavazzoni, D. Ceresoli, G. Chiarotti, M. Cococcioni, I. Dabo *et al.*, *J. Phys. Condens. Mat.*, 2009, **21**, 395502.
42 P. E. Blöchl, *Phys. Rev. B*, 1994, **50**, 17953.
43 N. Marzari, D. Vanderbilt, A. De Vita and M. C. Payne, *Phys. Rev. Lett.*, 1999, **82**, 3296.
44 N. Holzwarth, A. Tackett and G. Matthews, *Comput. Phys. Commun.*, 2001, **135**, 329.
45 S. G. Dale and E. R. Johnson, *Phys. Chem. Chem. Phys.*, 2016, **18**, 27326.
46 T. Björkman, A. Gulans, A. V. Krasheninnikov and R. M. Nieminen, *Phys. Rev. Lett.*, 2012, **108**, 235502.
47 D. Singh, H. Krakauer, C. Haas and W. Pickett, *Nature*, 1993, **365**, 39.
48 S. G. Dale, A. Otero-de-la Roza and E. R. Johnson, *Phys. Chem. Chem. Phys.*, 2014, **16**, 14584.
49 J. P. Perdew and A. Zunger, *Phys. Rev. B*, 1981, **23**, 5048.
50 Y. Zhang and Y. W, *J. Chem. Phys.*, 1998, **109**, 2604–2608.
51 W. Yang, Y. Zhang and A. P. W, *Phys. Rev. Lett.*, 2000, **84**, 5172.
52 P. Mori-Sanchez, A. J. Cohen and W. Yang, *J. Chem. Phys.*, 2006, **125**, 201102.
53 A. Ruzsinszky, J. P. Perdew, G. I. Csonka, O. A. Vydrov and G. E. Scuseria, *J. Chem. Phys.*, 2006, **125**, 194112.
54 A. Ruzsinszky, J. P. Perdew, G. I. Csonka, O. A. Vydrov and G. E. Scuseria, *J. Chem. Phys.*, 2007, **126**, 104102.
55 J. P. Perdew, A. Ruzsinszky, L. A. Constantin, J. Sun and G. I. Csonka, *J. Chem. Theory Comput.*, 2009, **5**, 902.
56 A. Ruzsinszky and J. P. Perdew, *Comput. Theor. Chem.*, 2011, **963**, 2.
57 E. Ruiz, D. R. Salahub and A. Vela, *J. Phys. Chem.*, 1996, **100**, 12265.
58 T. M. Henderson, B. G. Janesko and G. E. Scuseria, *J. Phys. Chem. A*, 2008, **112**, 12530.
59 A. Dreuw, J. L. Weisman and M. Head-Gordon, *J. Chem. Phys.*, 2003, **119**, 2943.
60 M. J. G. Peach, A. J. Cohen and D. J. Tozer, *Phys. Chem. Chem. Phys.*, 2006, **8**, 4543.
61 E. R. Johnson and A. D. Becke, *J. Chem. Phys.*, 2008, **128**, 124105.
62 A. J. Cohen, P. Mori-Sánchez and W. Yang, *J. Chem. Phys.*, 2007, **126**, 191109.
63 A. J. Cohen, P. Mori-Sánchez and W. Yang, *J. Chem. Phys.*, 2008, **129**, 121104.
64 T. Heaton-Burgess and W. Yang, *J. Chem. Phys.*, 2010, **132**, 234113.
65 D. Jacquemin, A. Femenias, H. Chermette, I. Ciofini, C. Adamo, J. M. Andre and E. A. Perpete, *J. Phys. Chem. A.*, 2006, **110**, 5952.
66 D. Jacquemin, E. A. Perpete, G. Scalmani, M. J. Frisch, R. Kobayashi and C. Adamo, *J. Chem. Phys.*, 2007, **126**, 144105.
67 G. Sini, J. S. Sears and J.-L. Bredas, *J. Chem. Theory Comput.*, 2011, **7**, 602.
68 S. N. Steinmann, C. Piemontesi, A. Delacht and C. Corminboeuf, *J. Chem. Theory Comput.*, 2012, **8**, 1629.
69 X. Zheng, M. Liu, E. R. Johnson, J. Contreras-García and W. Yang, *J. Chem. Phys.*, 2012, **137**, 214106.
70 E. R. Johnson, M. Salamone, M. Bietti and G. A. DiLabio, *J. Phys. Chem. A.*, 2013, **117**, 947.
71 S. R. Whittleton, X. A. S. Vazquez, C. M. Isborn and E. R. Johnson, *J. Chem. Phys.*, 2015, **142**, 184106.
72 A. D. Becke, *J. Chem. Phys.*, 1993, **98**, 1372.
73 A. D. Becke, *J. Chem. Phys.*, 1993, **98**, 5648.
74 P. M. W. Gill, R. D. Adamson and J. A. Pople, *Mol. Phys.*, 1996, **88**, 1005.
75 T. Leininger, H. Stoll, H.-J. Werner and A. Savin, *Chem. Phys. Lett.*, 1997, **275**, 151.
76 H. Iikura, T. Tsuneda, T. Yanai and K. Hirao, *J. Chem. Phys.*, 2001, **115**, 3540.
77 T. Yanai, D. P. Tew and N. C. Handy, *Chem. Phys. Lett.*, 2004, **393**, 51.
78 J. G. Angyán, I. C. Gerber, A. Savin and J. Toulouse, *Phys. Rev. A*, 2005, **72**, 012510.
79 B. G. Janesko and G. E. Scuseria, *J. Chem. Phys.*, 2008, **128**, 244112.
80 M.-C. Kim, E. Sim and K. Burke, *Phys. Rev. Lett.*, 2013, **111**, 073003.
81 P. Mori-Sanchez, A. J. Cohen and W. Yang, *J. Chem. Phys.*, 2006, **124**, 091102.
82 R. Baer, E. Livshits and D. Neuhauser, *Chem. Phys.*, 2006, **329**, 266.
83 T. Stein, J. Autschbach, N. Govind, L. Kronik and R. Baer, *J. Phys. Chem. Lett.*, 2012, **3**, 3740.
84 L. Kronik, T. Stein, S. Refaely-Abramson and R. Baer, *J. Chem. Theory Comput.*, 2012, **8**, 1515.
85 E. Kraisler and L. Kronik, *Phys. Rev. Lett.*, 2013, **110**, 126403.
86 X. A. Sosa Vazquez and C. M. Isborn, *J. Chem. Phys.*, 2015, **143**, 244105.
87 E. R. Johnson, M. Salamone, M. Bietti and G. A. DiLabio, *J. Phys. Chem. A.*, 2013, **117**, 947.
88 E. Riedo, E. Gnecco, R. Bennewitz, E. Meyer and H. Brune, *Phys. Rev. Lett.*, 2003, **91**, 084502.
89 G. Gao, R. J. Cannara, R. W. Carpick and J. A. Harrison,

Langmuir, 2007, **23**, 5394.
90 M. Chandross, C. D. Lorenz, M. J. Stevens and G. S. Grest, *Langmuir*, 2008, **24**, 1240.
91 I. Szlufarska, M. Chandross and R. W. Carpick, *Journal of Physics D: Applied Physics*, 2008, **41**, 123001.
92 Note that there was an error in the conversion from meV/atom to meV $Å^{-2}$ in Figure 2 of Ref. 2. The PW86PBE-XDM maximum-energy sliding barriers are 4.26, 5.49, and 13.58 meV/atom, which are correctly converted to 1.63, 2.01, and 4.71 meV $Å^{-2}$ for graphite, BN, and MoS_2, respectively, using the computed areas.
93 J. P. Perdew and Y. Wang, *Phys. Rev. B*, 1986, **33**, 8800.
94 The sliding barriers from the base DFT functional alone (at the XDM-corrected geometries) are -0.01, 0.20, -0.98 meV $Å^{-2}$ for graphite, BN, and MoS_2, respectively.
95 M. J. Wagner and J. L. Dye, *Annu. Rev. Mater.*, 1994, **25**, 223.
96 S. Grimme, *J. Comput. Chem.*, 2006, **27**, 1787.
97 J. Klimeš, D. R. Bowler and A. Michaelides, *Phys. Rev. B*, 2011, **83**, 195131.
98 C. Adamo and V. Barone, *J. Chem. Phys.*, 1999, **110**, 6158–6170.
99 A. D. Becke and E. R. Johnson, *J. Chem. Phys.*, 2006, **124**, 014104.
100 E. R. Johnson, *J. Chem. Phys.*, 2011, **135**, 234109.
101 M. S. Christian, A. Otero-de-la Roza and E. R. Johnson, *J. Chem. Theor. Comput.*, 2016, **12**, 3305.
102 D. Sulzer, P. Norman and T. Saue, *Mol. Phys.*, 2012, **110**, 2535.
103 S. G. Porsev and A. Derevianko, *J. Exp. Theor. Phys.*, 2006, **102**, 195.
104 O. Allard, C. Samuelis, A. Pashov, H. Knöckel and E. Tiemann, *Eur. Phys. J. D*, 2003, **26**, 155.
105 C. Vidal, *J. Chem. Phys.*, 1980, **72**, 1864.
106 R. J. Le Roy and R. D. Henderson, *Mol. Phys.*, 2007, **105**, 663.
107 R. Moszynski, G. Łach, M. Jaszuński and B. Bussery-Honvault, *Phys. Rev. A*, 2003, **68**, 052706.
108 B. Bussery-Honvault, J.-M. Launay and R. Moszynski, *Phys. Rev. A*, 2003, **68**, 032718.
109 M. Mérawa, C. Tendero and M. Rérat, *Chem. Phys. Lett.*, 2001, **343**, 397.
110 J. Mitroy and J.-Y. Zhang, *Phys. Rev. A*, 2007, **76**, 032706.
111 V. G. Ruiz, W. Liu, E. Zojer, M. Scheffler and A. Tkatchenko, *Phys. Rev. Lett.*, 2012, **108**, 146103.
112 A. Becke and M. Roussel, *Phys. Rev. A*, 1989, **39**, 3761.
113 F. L. Hirshfeld, *Theor. Chim. Acta*, 1977, **44**, 129.